BULLETIN OF THE POLISH ACADEMY OF SCIENCES
TECHNICAL SCIENCES, Vol. 73(1), 2025, Article number: e152706
DOI: 10.24425/bpasts.2024.152706

Determination of wind force acting on an object in the shape of a bent pipe

Agnieszka PADEWSKA-JURCZAK[1]*, **Zbigniew BULIŃSKI**[2], and **Tomasz KRYSIŃSKI**[2]

[1] Department of Mechanics and Bridges, Faculty of Civil Engineering, Silesian University of Technology, Akademicka 5, 44-100 Gliwice, Poland
[2] Institute of Thermal Technology, Faculty of Energy and Environmental Engineering, Silesian University of Technology, Konarskiego 18, 44-100 Gliwice, Poland

Abstract. The aim of the paper is to determine the aerodynamic forces acting on a torus-shaped structure fragment at high wind velocity which are impossible to obtain from the existing standard EN 1991-1-4 (the so-called wind standard). The most important problem is the correct modeling of turbulence and laminar-turbulent transition in the conditions of flow interference resulting from the presence of other obstacles. For this reason, forces are obtained by two methods: fluid-structure interaction (FSI, force transfer) and user-defined functions (UDF). Variations of the total aerodynamic lift force of the half of the torus with angle β and velocity of wind w, and the formula for estimating the horizontal force P_z perpendicular to drag force are presented. Additionally, useful engineering parameters (such as pressure distribution and air velocity field) are determined. The forces of wind influence on two cylinders and a torus-shaped object are obtained and compared.

Keywords: wind action; water slide; fluid-structure interaction (FSI); user-defined functions (UDF); finite volume method (FVM); finite element method (FEM).

NOMENCLATURE

CFD	–	computational fluid dynamics
DNS	–	direct numerical simulation
FEM	–	finite element method
FSI	–	fluid-structure interaction (force transfer)
FVM	–	finite volume method
Re	–	Reynolds number
UDF	–	user-defined functions
k-ϵ	–	turbulence model
k-ϵ/RNG	–	re-normalisation group k-ϵ turbulence model
k-ω	–	turbulence model
k-ω/SST	–	shear stress (SST) k-ω turbulence model
b [m]	–	diameter of the cross-section of the torus
c_p [–]	–	pressure coefficient
c_f [–]	–	force coefficient according to [1]
c_x [–]	–	drag coefficient
c_y [–]	–	lift coefficient
G [N]	–	weight of the structure
g_r [mm]	–	thickness
k [mm]	–	roughness of the cylinder wall
k [m^2/s^2]	–	turbulent kinetic energy
l [m]	–	length
p [Pa]	–	pressure
P_x [N]	–	drag force
P_y [N]	–	lift force
P_z [N]	–	horizontal force perpendicular to drag
q_p [kN/m^2]	–	peak velocity pressure
R [m]	–	radius of the torus
w [m/s]	–	velocity of wind
y [mm]	–	estimated first FVM element height
y^+ [–]	–	nondimensional wall distance
z [m]	–	height above ground
α [°]	–	angle that defines part of a torus
β [°]	–	yaw angle
γ [kN/m^3]	–	volume weight
Δ [%]	–	relative difference
δ [mm]	–	thickness of boundary layer
ρ [kg/m^3]	–	density
ω [1/s]	–	specific dissipation rate

*e-mail: agnieszka.padewska-jurczak@polsl.pl

Manuscript submitted 2024-03-15, revised 2024-10-17, initially accepted for publication 2024-11-06, published in January 2025.

1. INTRODUCTION

1.1. Motivation to take up research

The action of the wind is the dominant load for the water slide, especially when it is located in an open area, by a lake, or in the mountains. Its actual maximum values occur at high altitude, generating significant bending moments in the restraint of load-bearing columns (Fig. 1). This research is universal and can also

Fig. 1. Water slide in Gino Paradise Bešeňová in Slovakia

© 2025 The Author(s). This is an open access article under the CC BY license (http://creativecommons.org/licenses/by/4.0/)

be applied to other objects in the shape of a bent pipe. Calculating the wind flow is a complicated task that requires, among others, knowledge of the specific rules of setting boundary conditions, choosing the right model of turbulence, and precise formation of the FVM mesh in the area around the object wall in order to correctly reproduce changes in the velocity gradient in the boundary layer.

1.2. Objective of research

This paper is an introduction to the full analysis of the wind impact on the object in the shape of a bent pipe (e.g. water slide, pipelines, elements of bridges). At this stage, the research is limited to modeling its fragment (see e.g. [2–4]). The aim of the analysis is to test the possibility of a much faster estimation of wind loads acting on a fragment of a structure of a curved shape (e.g. a water slide) using a simplified model (in the shape of a torus). Wind forces results obtained by FSI (force transfer) and UDF were compared. The aim is to identify the most useful and fastest method of numerically designing structural elements in the shape of a bent pipe in terms of wind load. A calculation error is evaluated for this approach. Analyses present a study on the development and verification of numerical models of flow at high wind velocity around structural elements with a circular cross section and simple shape, allowing the determination of useful engineering parameters (such as aerodynamic forces, pressure distribution, and air velocity field). Especially, the influence of strong wind is considered, having velocity above 30 m/s, on the structures with complicated shape which to some extent are similar to torus. In such a situation strong wind inference caused by the flow around different parts of the same body appears. Difficulties in estimating the aerodynamic forces acting on objects of unusual shape result, inter alia, from the fact that the reference surfaces, e.g. an object in the shape of a half-torus set at different angles to the horizontal, as well as its fragments, do not correspond to the surfaces resulting from the projection of the object on a plane perpendicular to the direction of the wind velocity or the surface of the equivalent cylinder. The forces of wind influence on the cylinders and a torus-shaped object were determined and compared. Due to the fact that the Eurocode [1] does not cover the issues related to the wind load on structures with atypical shape, new formula is proposed. It was derived on the basis of the algorithm for calculating the force of wind on the cylinder perpendicular to the direction of airflow, described in the European standard [1], which provides detailed dependencies of the aerodynamic drag coefficient on the roughness of the cylinder surface and on the Reynolds number which is the ratio of inertial forces to viscous forces within a fluid. Depending on the type of external surface adopted by the designer, this coefficient may vary significantly. Analyses, also shown in previous papers [2–4], begin with the flow around a cylinder. This is the simplest object with a circular cross-section and at the same time the most studied in the literature (see, e.g. [5–7]) and newer papers: [8–10]. Based on this model, more complex models were analyzed, in the shape of half of a torus. In the article [11] simulations are presented for flow around pairs of circular cylinders at a Reynolds number of 3900. There are not many analyses in the literature on the impact of wind on a torus-shaped object. In the paper [12] the flow structure of a torus with an aspect ratio of three was scrutinized in a wind tunnel at the Reynolds numbers with values much smaller than in the present paper. Similarly in [13]. The study [14] explores the application of toroidal propellers in drone technology through comprehensive wind tunnel testing.

Because a fragment of a relatively rigid structure is analyzed, at the present stage of the study the potential problem of vortex-induced vibrations is omitted and mostly one-way force transfer is used. Such structures have a vertical static system, with horizontal cantilever or strutted beams connected to columns, and a steel bracing system. These issues will be discussed in the future. A selective review of recent research on vortex-induced vibrations of isolated circular cylinders and the flow and vibration of circular cylinders in tandem arrangement are presented in both [15–17] and [18, 19]. Additional results of the analyses were mentioned in [20]. Vortex excitation has also been investigated behind objects in the shape of a quarter of a torus or a whole torus, stationary or rotating around the central axis, e.g. in [21–23]. The mentioned papers deal with small numbers Re, unlike the present analyses. The determination of wind impact forces was not the purpose of the analyses presented therein.

1.3. Research methodology

The problem was solved both by using the coupled FVM for solving fluid flow problem and the FEM for solving structural problem. Hence, it was a fully coupled two-way FSI approach in which the Fluent ANSYS CFD (Computational Fluid Dynamics) solver was coupled with the Abaqus FEM solver. This approach was confronted with one-way interaction carried out through UDF on the ANSYS Fluent platform. Some calculations were carried out on the PL-Grid Infrastructure.

2. NUMERICAL MODELS OF AIRFLOW AROUND STRUCTURAL ELEMENTS

2.1. Calculations using FSI

The development and verification of models of wind flow around spatial elements in the shape of half of a torus, yawed at the angle β in the range 0–90° were shown in previous papers [2, 20, 24]. They also include the results of numerical analyses. The subject of analysis is the reactions of individual parts of the torus as a result of changes (e.g. pressure) in the flow characteristics. For this purpose, the object is divided into eight equal parts. One-way force transfer is assumed (fluid → structure). All parts were bonded together, without the possibility of slipping or separation, through contact (bonded contact). Geometry was created in the ANSYS DesignModeler. It is assumed that the object does not deform under the influence of wind. In the solver, individual rigid parts are represented by a single point, which transfers inertial properties, and a discretized surface which is the geometry of the object. The shell thickness is assumed to be 0.01 m, but setting the shell thickness factor to 0 causes the physical thickness and node offset from the center cross-section of the surface to be ignored. The cutout in the shape of a torus in the airflow model and the model in the mechanical

part perfectly match with respect to the arrangement in space. The radius of the torus $R = 3.0$ m and the diameter of the cross-section of the torus $b = 1.0$ m. Figures 2 and 3 show a general view, boundary conditions, directions of aerodynamic forces, division into blocks, and FVM mesh of the numerical model of airflow around the object in the shape of half of the torus, made in the ANSYS package.

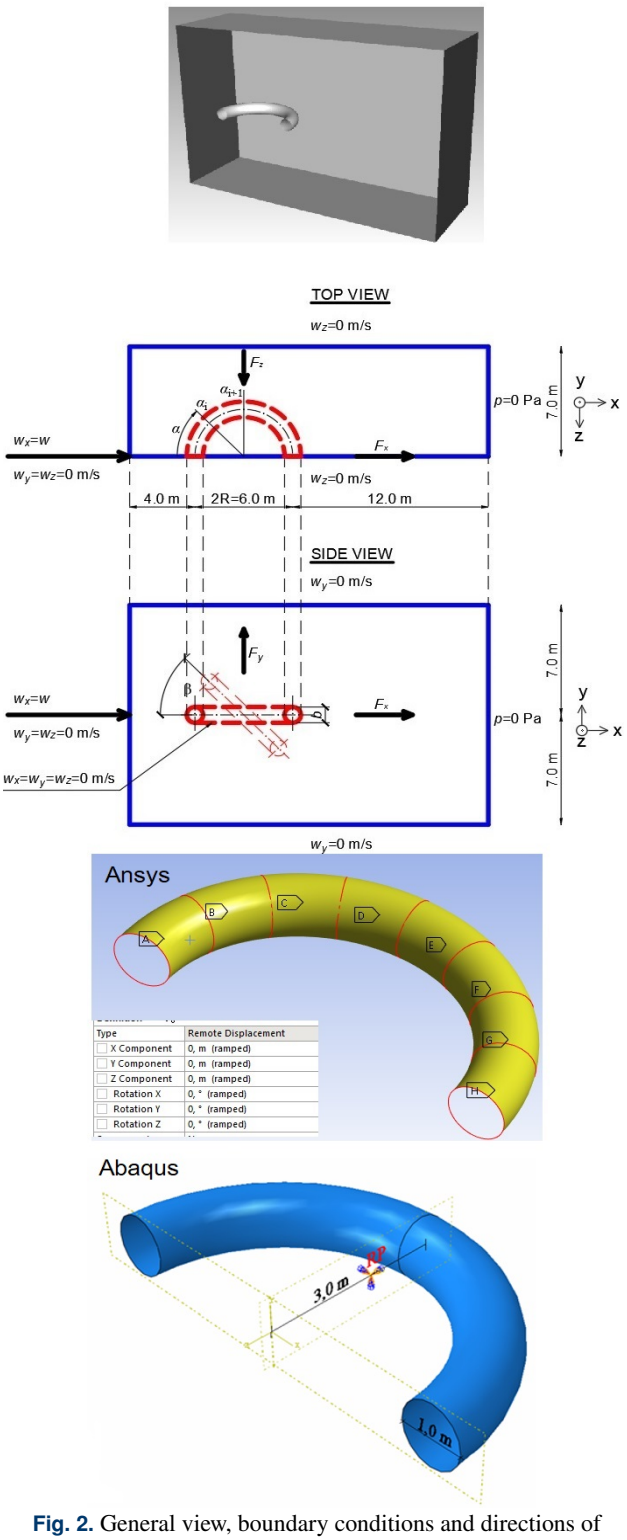

Fig. 2. General view, boundary conditions and directions of aerodynamic forces in a model of flow around half of a torus

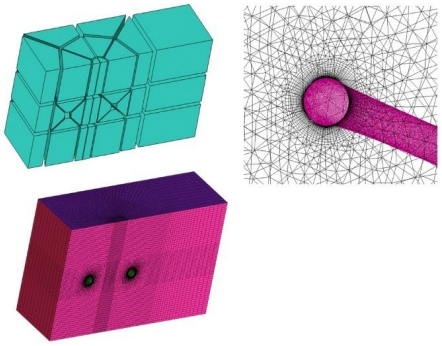

Fig. 3. Division into blocks and FVM mesh of the model of flow around a curved pipe

The boundary layer is meshed in an analogous manner to the case of the base model, in the shape of a single cylinder (see [4]). If it was not possible to divide into regular subareas, a hybrid mesh was used, consisting of a regular mesh in the boundary layer and triangular and tetrahedral mesh elements in an area at a greater distance from the object wall. Most often, the calculations were performed at hurricane speed. When a storm maximum sustained winds reach 33 m/s, it is called a hurricane. The Saffir-Simpson Hurricane Wind Scale is a 1 to 5 rating, or category, based on a hurricane maximum sustained winds. The higher the category, the greater the potential for property damage from the hurricane. In the case of the aerodynamic drag of half of the torus set horizontally, at a hurricane wind velocity, the relative differences between the results obtained using the regular and hybrid mesh, depending on the angle α, ranged from 0.6% to 5%, and in the case of a horizontal force perpendicular to the drag force – from 0.5% to 5%. Nonstructural meshes were also used, made of prisms (wedges) near the pipe wall and tetrahedra in an area at a greater distance from it (see Fig. 2). The comparison of the results obtained with the use of the hybrid and non-structural mesh for the model of a half of the torus yawed from the horizontal surface by 22.5° showed that the forces P_x and P_z did not differ by more than 2%. The size of the mesh elements on the object surface of 0.04 m was chosen such that the number of elements around the pipe outlet corresponded to the number of elements around the pipe outlet in the hybrid and structured mesh (96 elements in total around the outlet of the cross-section of the pipe).

In Fig. 4, the FEM mesh of the curved pipe model divided into eight parts is shown. FEM and FVM grids on the wall of the object and near the cutout are sufficiently similar, so that the force vectors transferred from the model of wind flow act exactly perpendicularly to the finite elements of the structure, which is particularly important in the case of the surface of a curved shape. The mesh consists of over 12 000 SHELL181 surface elements (four node elements with six degrees of freedom at each node). In Abaqus there are nondeformable, three-dimensional, four-node linear elements (R3D4). The common surface of the fluid and the object is declared as a boundary condition. In the analyses presented in this paper, 100% of the nodes were successfully mapped, which could be read from the diagnostic note in the Static Structural program at the end of the iteration.

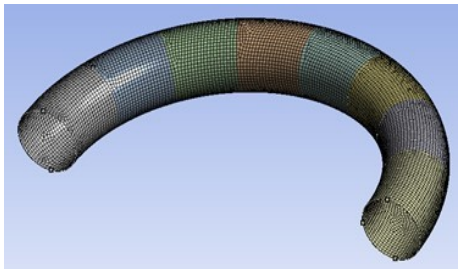

Fig. 4. FEM grid of a model of a bent pipe divided into eight parts

Air with a uniform velocity profile enters the domain through a front surface (inlet) and flows out through the back surface (outlet), where the pressure is equal to that of the atmosphere. Symmetry (or far-field in Abaqus/CFD), which is essentially a wall with slip condition, is chosen for the top and bottom boundaries to reduce the computational time. The roughness of the cylinder wall is considered with a value of $k = 0.15$ mm, which corresponds to the surface of a fiberglass laminate. As well as adjusting to zero air velocity of the fluid in the immediate vicinity of the surface of the object (No Slip Wall). An important issue is the selection of an appropriate size of a domain while bearing in mind that the calculations are complex, requiring considerable computing power. The dimensions of the computational model are chosen so that the inlet, outlet, and symmetry or the far-field boundaries are far enough from the object to avoid any boundary effects, according to [25–27].

When the calculation area was enlarged twice in the direction of the $0x$ and $0z$ axes, at wind velocity $w = 33.5$ m/s, the P_x and P_z components of the total wind force on the entire half-torus-shaped object were reduced by approximately 6% and 3%, respectively. On the other hand, increasing the height of the computational domain of the air flow by 8 m at the velocity of 15 m/s near the torus yawed at an angle of 15° to the horizontal surface resulted in the reduction of the P_x force by 1%, the P_z force by 3% and the P_y force by 3%. To verify the possibility of testing the wind force of the whole torus with the model of its half, using the symmetry condition, the whole torus located horizontally was analysed, subjected to a hurricane wind velocity $w = 33.5$ m/s. The total force P_x acting on the entire torus turned out to be only 2% smaller than the double total force acting on a half of the torus, and the total force P_z – as predicted – had a value of zero. Larger discrepancies were observed in the case of the 8^{th} part and its mirror image of the entire torus model. Due to the randomness and turbulence of the flow in this place, the difference in P_x forces in these fragments was 12%, P_z forces – 13%, and in the remaining parts it was not greater than 0–5%. The final summary values of the aerodynamic forces of the half and the whole torus remained consistent.

The fluid was modeled as an incompressible Newtonian fluid. Finally, the following options were selected (among others):

- pressure-based solver,
- second-order upwind interpolation scheme, and
- transient flow.

The appropriate time-step size of the calculations was also estimated. The justification for choosing such options is shown in [3]. Exactly the same approach was used. Re values applied in the calculations were in the critical and supercritical range of the turbulent flow. They were determined in part on the basis of [1]. An analysis of turbulence models was made. Quoting [25]: "The shear stress (SST) k-ω model was developed by [28] to effectively blend the robust and accurate formulation of the k-ω model in the near-wall region with the freestream independence of the k-ϵ in the far field. To achieve this, the k-ϵ model is converted into k-ω formulation. These features make the SST k-ω model more accurate and reliable for a wider class of flows (e.g. adverse pressure gradient flows, airfoils, transonic shock waves) than the standard k-ω model." When using the LES method, the problem was setting the surface roughness. In the ANSYS package, it was not possible to set the height of the roughness of the water slide wall. At the same time, the direct numerical simulation (DNS) method requires the use of computers with enormous computing power. It would be impossible to analyze the cases in the present and later papers with even more complex shapes using this method.

Verification of the numerical model was made on the example of a simplified model in the shape of a cylinder. The FVM grid in the vicinity of the object was the same as in the case of a torus. In the calculations presented here it is assumed that the turbulent kinetic energy and the specific dissipation rate are equal respectively to: $k = 60.8$ m^2/s^2 and $\omega = 930.2$ 1/s for the thickness of boundary layer $\delta = 3$ mm and hight above ground $z = 10.0$ m. From wide range calculations it turned out that the drag coefficient, which is used to quantify the drag or resistance of an object in a fluid environment, such as air, was almost insensitive to k and ω parameter values as much as the tenfold reduction of these values caused increasing of the average value of the drag coefficient of just 1.1%. For this reason, it was decided to change individual cases due to the wind velocity declared as the boundary condition instead of the parameters of the turbulence models.

The integral time-average value of the drag coefficient using (1) the standard k-ω and k-ϵ/RNG turbulence models resulted in $c_x = 0.64$ and (2) the k-ω/SST or DES models – $c_x = 0.59$. Figure 5 represents the time series of drag coefficients at a wind velocity $w = 33.5$ m/s by using two of the previously mentioned exemplary turbulence models, as well as the lift coefficients c_y. Its average value is equal to zero. The amplitude of oscillation is 0.3. This value is consistent with the results obtained in the wind tunnel and described in [29].

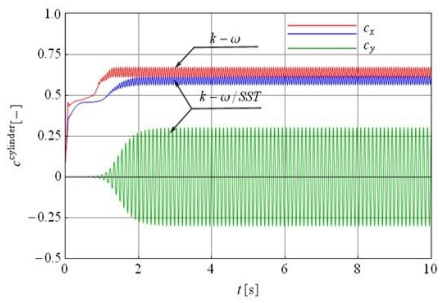

Fig. 5. Variation of the drag and lift coefficient of the cylinder during the first 10 s at $w = 33.5$ m/s obtained using different turbulence models

Table 1 shows, depending on the velocity of wind flow and Re number, the nondimensional wall distance y^+, adopted according to [30–32]. In the mentioned references, among others, possible to use ranges of values y^+ are included, corresponding to each zone of the viscosity-affected region. The paper [33] also reports on the development of a refined wall function strategy to model turbulent flow on rough surfaces. The validation results suggest that the proposed extension is successfully applicable to a wide range of attached and separated turbulent flows over fine-grained rough surfaces.

Table 1
Re values and FVM grid refinements

w [m/s]	11 (strong breeze)	15 (high wind)	22 (strong gale)	33.5 (hurricane)
Re [–]	$7.3 \cdot 10^5$	10^6	$1.5 \cdot 10^6$	$2.2 \cdot 10^6$
y^+ [–] minimum	6	7	10	14
y^+ [–] coarse mesh	50	63	90	135
y^+ [–] fine mesh	6	7	40	50

The values of the Reynolds number are characterized by equation:

$$\mathrm{Re} = \frac{b \cdot w}{\nu} = \frac{1 \cdot w}{15 \cdot 10^{-6}} \quad [-], \tag{1}$$

where: $b = 1$ m is a diameter of a cylinder and ν – kinematic viscosity according to [34].

The estimated first FVM element height equals:

$$h = 2y = \frac{2\sqrt{74}}{\mathrm{Re}^{13/14}} b y^+ = 3 \text{ mm} \tag{2}$$

using a coarse mesh. This value can be estimated using the calculator available at https://www.cfd-online.com. Minimal value of y^+ is shown in Table 1 (assuming that the value of y is slightly greater than that of k). It also includes the maximum value of y^+ (a fine mesh) for which the drag coefficient remains almost unchanged, it means that the difference between solutions for different small y^+ is less than 5%. Larger values of y^+ than those listed in Table 1 do not apply in these analyses.

A structural type of FVM mesh was made. Models have significantly lower computational requirements (and coarse mesh) when using wall functions. Then, the first computational node is placed in the fully turbulent inner region, and suitable assumptions about how the near-wall velocity profile behaves are made to obtain the wall shear stress. In this paper, the production limiter option was used. The wall boundary conditions for the equation in the models were treated in the same way as the equation was treated when enhanced wall treatments were used. The maximum value of a c_x coefficient for a model with a coarse mesh is comparable (lower by about 5%) to the force coefficient value given in the European code [1]. Following the adoption of more restrictive rules of discretization, the drag coefficient value was shown to be lower by about 30%, and it is consistent with the results measured in the cryogenic wind tunnel and described in [5].

Figure 6 indicates that $y^+ = 135$ for $w = 33.5$ m/s (except for the front and the trailing surface of the cylinder, where stagnation of air occurs), and 50 at $w = 11$ m/s. It is marked with an upper line. Furthermore, it does not drop significantly below 50 and 6 (a lower line). Therefore, it can be concluded that the resolution of the near-wall mesh is acceptable in both cases. The dotted line represents the y^+ values on the wall of the cylinder as read when the aerodynamic force reached the mean value. Due to the presence of turbulence, these values are different in the upper and lower parts of the cylinder.

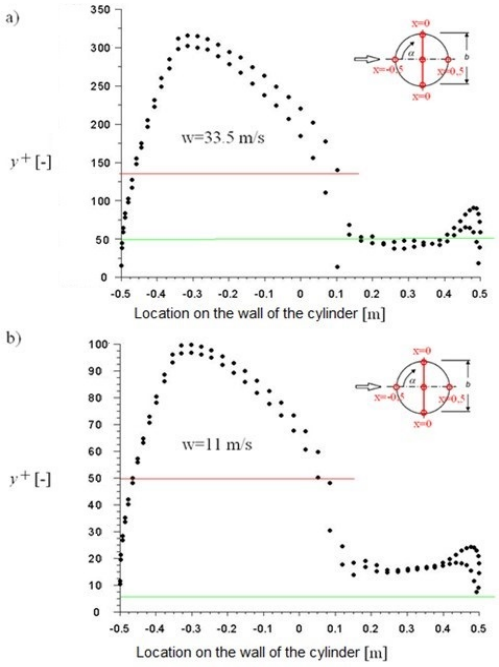

Fig. 6. y^+ distribution on the wall of the cylinder at $w = 33.5$ m/s and $w = 11$ m/s

The distribution of velocity vectors near the cylinder wall is shown in Fig. 7. Behind the cylinder is the region in which the air recirculates. The flow is not symmetrical and no regular path is formed. This flow characteristic is in accordance with Fig. 7.16 in [35] in the critical range of Re. The point of separation of the boundary layer is determined from the distribution of static pressure and shear stress on the wall of the cylinder, and the velocity vector field around the wall. It occurs at an angle of approximately 110°. A similar angle was determined experimentally and described in [6]. Furthermore, a very good agreement is observed between the results of the mean pressure distribution on the surface of the cylinder at $\mathrm{Re} = 2.2 \cdot 10^6$ in this paper (Fig. 8) and the sets of experimental data described in [6, 36, 37], and numerical results in [34]. The dotted line represents the pressure coefficients on the wall of the cylinder as read when the aerodynamic force reached the mean value. Due to the presence of turbulence, the pressure is different in the upper and lower parts of the cylinder. Therefore, the mean value

was calculated and marked with a solid line. Good agreement is observed between the results of the mean pressure distribution on the cylinder surface in this paper and the experimental data described in the European standard [1]. A similar distribution of pressure coefficients was obtained for the other Re numbers: $7.3 \cdot 10^5$, 10^6, and $1.5 \cdot 10^6$.

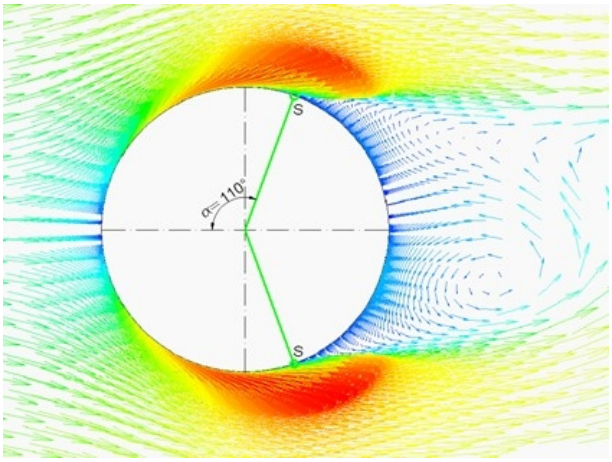

Fig. 7. Velocity vectors near the cylinder wall and the boundary layer separation point for Re = $2.2 \cdot 10^6$

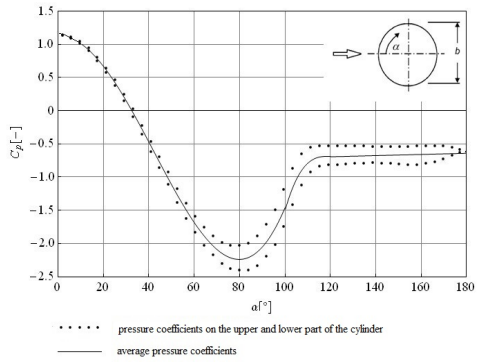

Fig. 8. Distribution of average values of pressure coefficient c_p on the wall of the cylinder

Additional FSI analysis was performed on the Abaqus package to determine the aerodynamic forces. FSI represents a class of multiphysics problems in which fluid flow affects compliant structures, which in turn affects fluid flow [38]. It is the interaction between the Euler fluid and the Lagrange construction, which are in contact through a common surface (co-simulation boundary). A procedure enabling the transfer of data by both solvers at each time step (co-simulation) was used. Considering the turbulence model k-ω/SST in ANSYS Fluent, a value of drag coefficient close to the value resulting from the application of the model k-ϵ/RNG in the Abaqus package was obtained, regardless of the method specified in [4].

Following the adoption of all previous rules, the problem converged. Residuals were decreased by three orders of magnitude. The net mass imbalance was less than 0.2% of the net flux through the domain. This means that when the present models were used, reliable results were obtained.

2.2. Calculations using UDF

The assumption that the deformations of the structure are negligible facilitates limiting the analysis to a one-way FSI. However, the procedure for transfers from ANSYS Fluent external wind loads acting on a fragment of a water slide requires the inclusion of another module in the ANSYS Workbench package - Static Structural. Both models (CFD and mechanical part) must perfectly match each other in terms of orientation in space. Implementing the FEM mesh on the wall of the object and the declaration of contact between the eight parts of a half of a torus are problematic. The wind force vectors transferred from a model of wind flow must act exactly perpendicularly to the finite elements of a structure with a curved shape.

UDFs were written in the programming language C. They were dynamically loaded with the ANSYS Fluent solver in the form of macros, which resulted in access to calculated fields of variables and to the geometry of an object. The functions have been compiled in the Fluent program using Microsoft Visual Studio. As a result, shared libraries that were connected to the entire solver were created.

The subject of analysis is the reactions of different parts of the torus due to changes in the flow characteristics, for example, pressure. Partial results have already been presented in earlier papers [2–4]. Figure 9 shows the pressure, velocity, and streamline distributions in the middle cross-section of the flow model around half of the torus at the time when the resulting aerodynamic drag force reaches the mean value, presented in other papers. The largest absolute value of the lateral force (side) directed outward relative to the curvature axis of the torus appears in the fifth and sixth parts of the torus (see Fig. 1; the angle α of approximately 110°). Its source is a big difference between the air velocity in the region in the 'eye' (center) of the torus and on the sides. The effect is analogous to the lift force obtained by airfoils. Noorani [39] observed that for strong curvature a distinct bulge appears close to the center of the pipe in fully developed, statistically steady turbulent flow in straight and curved pipes (torus fragment) at moderate Reynolds numbers.

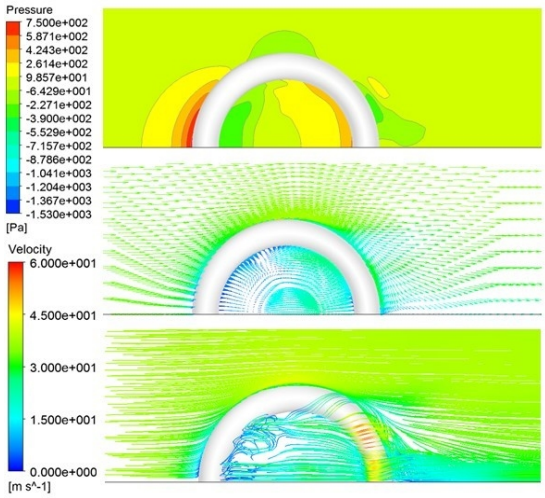

Fig. 9. Distribution of pressure, velocity and streamlines in the middle cross-section of a model of flow around half of the torus at $\beta = 0°$ and $w = 33.5$ m/s

Figure 10 shows a static pressure distribution on the wall of the object in the shape of half of the torus yawed from the horizontal surface at an angle of 22.5°, which is more similar to a fragment of the water slide. It is like the pressure distribution on the wall of half of a torus positioned horizontally.

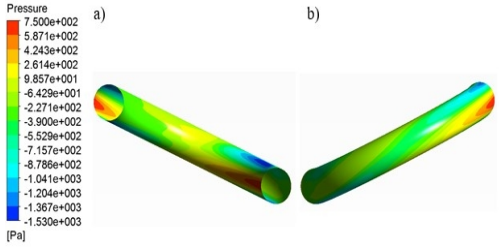

Fig. 10. Pressure distribution on a surface of a torus yawed from the horizontal surface by an angle 22.5°: (a) front view and (b) rear view

The authors' own program code compiled in ANSYS Fluent allowed the calculation of the viscous forces, pressure forces, and total forces in a direction 0*X* on different parts of the surface of a torus positioned horizontally at hurricane wind velocity. The results were automatically saved to a text file at each iteration. They were used to verify force transfer. Table 2 presents a comparison of drag forces acting on individual parts of half of the torus obtained by the UDF and FSI methods after the first second of flow. The resulting forces acting on the whole object in the shape of half of a torus are also compared. In the 'UDF' column, the values of forces are presented as the sum of viscosity and pressure forces. This also illustrates how little importance viscous forces have in turbulent flows considered in this paper. In the program Static Structural, it is not possible to separate these forces. The force values are for illustrative purposes only, to verify the FSI analysis because they were read out after only one second of flow.

Table 2

Comparison of the results of the total forces acting on individual parts of a torus after the first second of flow obtained by UDF and FSI methods [N]

No. of a part of a half torus	UDF [N]	FSI [N]	Δ [%]
1	6.2 + 277.7 = 283.9	284.2	–0.1
2	8.6 + 288.8 = 297.4	297.8	–0.1
3	6.3 + 149.7 = 156.0	155.8	+0.1
4	4.8 + 45.4 = 50.3	50.6	–0.6
5	7.2 - 42.3 = -35.1	–34.2	+2.6
6	8.4 - 9.6 = -1.14	–0.79	+44.3
7	9.0 + 176.7 = 185.7	185.1	+0.3
8	9.4 + 350.9 = 360.4	358.3	+0.6
Σ	1297.4	1296.3	+0.1

Results obtained by UDF and FSI methods are sufficiently compatible, given that during force transfer from the Fluent to Static Structural, numerical errors are generated even though the object is stiff and immovable. Differences between very small, close to zero force values in the sixth part of half of the torus can be omitted in engineering applications. Results of the final calculations of the resultant forces P_x and P_z, described in [2] and using FSI, are presented in Fig. 11. The points highlighted on the curves, e.g. in the case of the angle $\alpha = 67.5°$, determine the sum of reactions from the first, second and third part of half of the torus, and the reaction for the angle $\alpha = 180°$ is the sum of the reaction [3]. The results for the remaining values of wind velocity are also presented there. Figure 11 also shows dimensionless values of the components of the aerodynamic force. They denote the ratio of the value of the aerodynamic force component obtained from numerical analysis to the force that can be calculated analytically. This graph shows that these forces differ up to three times. Therefore, a function to correct for these force values should be applied.

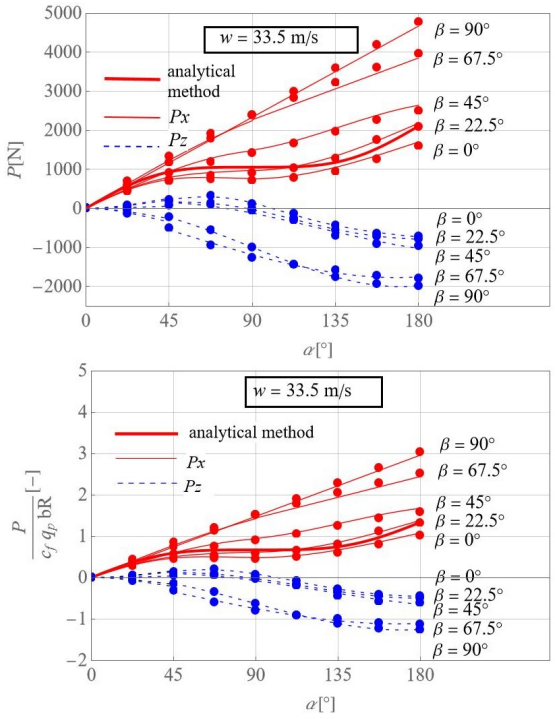

Fig. 11. Variations of the aerodynamic forces P_x and P_z with the α and β angle using FSI – real and dimensionless values

These papers [2] and [3] also present the variability of the values of the aerodynamic force components of the half-torus-shaped object depending on the angle β and the wind velocity w (Fig. 12). In [2] the procedure for deriving the function marked in Fig. 11 as an 'analytical method' is shown. It was determined for a horizontally oriented torus. This figure also shows dimensionless values of the components of the aerodynamic force, similar to Fig. 11, for each wind velocity analysed in this paper. This graph also shows that these forces differ by up to three times. Therefore, in this case, the function of correcting the results should also be applied.

Based on the graphs shown in Fig. 12, it can be shown that the P_x component of the wind load on half of the torus can be

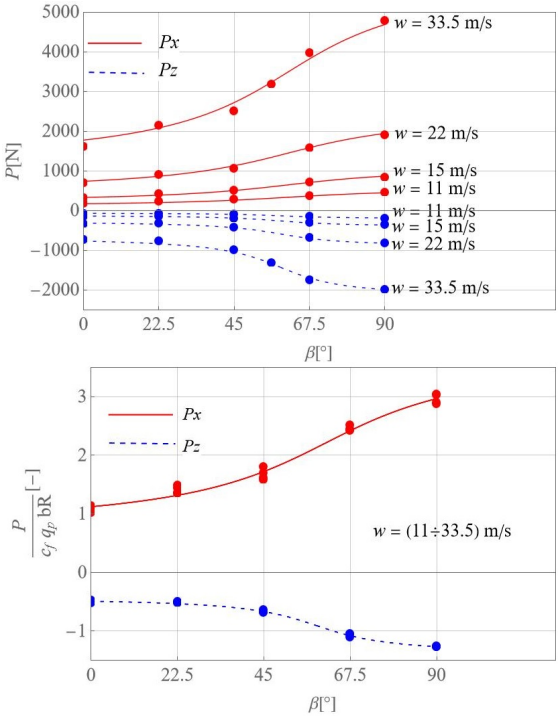

Fig. 12. Variations of the total aerodynamic forces P_x and P_z with angle β and velocity of wind w using FSI – real and dimensionless values

estimated from the formula:

$$P_x = c_f q_p bR\,[2.21 - 0.97 \arctan(2.098 - 0.034\beta)]\,, \qquad (3)$$

where

$$q_p = \frac{\rho w^2}{2}\,, \qquad (4)$$

according to [1].

The aerodynamic coefficient c_f can be assumed as for a circular cylinder according to [1]. This is because all the analyses started with the case of a circular cylinder with the same diameter as the torus. All parameters of the numerical model of the cylinder and the torus are also the same. Additionally, the FVM mesh was selected so that the c_f values for the circular cylinder were the same as those given in [1]. Table 3 shows the values of this coefficient used for calculations, as well as the values of q_p.

Table 3
List of parameters for calculating the wind force

w [m/s]	11	15	22	33.5
q_p [Pa]	75.6	140.6	302.5	701.4
c_f [–]	0.66	0.69	0.72	0.75

The first step was to obtain the results of the aerodynamic forces depending on the β angle and wind velocity. These results were approximated by the function given in equations (3) or (5). Angle β is expressed in degrees. This force must be doubled for the entire torus. The formula for estimating the horizontal force P_z perpendicular to the drag force is:

$$P_z = c_f q_p bR\,[-0.91 + 0.31 \arctan(4.10 - 0.07\beta)]\,. \qquad (5)$$

For the entire torus, this force is set to zero.

Both equations have already been presented in [2]. This article also mentioned that formulas (2) and (4) apply to β angles from 0 to 90°. In other cases, the symmetry of the relationship with respect to the vertical axis β = 90º is used. The errors in the approximation of the P_x force range from –1% to +11%. They refer to the highest and lowest wind velocity at angles β of 0° and 22.5°, respectively. Regarding the force P_z, these errors range from 7% to 9% at the two highest values of velocity and angle $\beta = 45°$.

The values of the P_y component force (Fig. 13), obtained for the purposes of the present paper, reach values close to even 62% of the P_x force. For the whole toruses, these forces must be doubled.

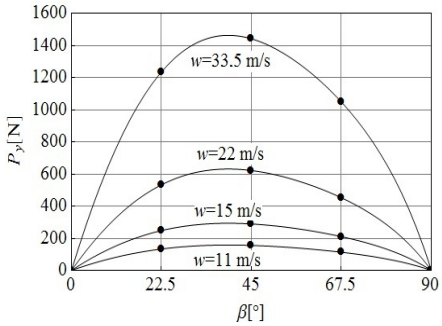

Fig. 13. Variations of the total aerodynamic lift force of the half of the torus with angle β and velocity of wind w using FSI

However, comparing them with the weight of a fragment of an actual half-torus-shaped water slide made of laminate with a thickness g_r = 1 cm and volume weight γ = 20 kN/m^3:

$$G = \gamma \frac{1}{2}\left(4\pi^2 \frac{b}{2} R\right) g_r\,, \qquad (6)$$

it turned out that they almost did not matter in the assessment of structural safety. As mentioned earlier, the topics related to vortex excitation and dynamic interactions go beyond this stage of the analysis. The results presented were obtained to facilitate the estimation of aerodynamic forces on the basis of the European standard. With this assumption, the maximum values of the drag coefficient of the cylinder perpendicular to the direction of the wind flow, calculated using the Fluent program, were comparable to those contained in the standard [1], determined at the maximum value of the velocity pressure. The average values of these coefficients, used in these analyses, were approximately 5% lower than the standard values. As shown in the previous parts of this paper, in the paper [5], based on tests in a wind tunnel, the actual values of the drag coefficient for a straight cylinder are even 30% lower than the standard. For these reasons, the forces obtained by the numerical method, with

more restrictive rules for the discretization of the boundary layer by reducing the height of the elements closest to the obstacle wall, would be correspondingly smaller than those shown in the graphs. Formulas (2) and (4) are therefore engineering estimates of the aerodynamic forces acting on objects in the shape of a half or a whole torus.

The obtained dependencies were verified using additional models of the flow around the halves of a horizontal torus: 1) with a radius $R = 6$ m and a diameter $b = 1$ m and 2) $R = 11$ m and $b = 0.8$ m. The results are as follows: the aerodynamic drag resulting from the application of equation (2) is greater than P_x force obtained from the numerical analysis by approx. 1) 8% and 2) 13%. On the other hand, P_z force hardly changes after increasing the radius. Therefore, formula (4) should be corrected to the form:

$$P_z = c_f q_p b3\left[-0.91 + 0.31 \arctan\left(4.10 - 0.07\beta\right)\right]. \quad (7)$$

However, at this stage of the research, the obtained relationships are appropriate for curved pipes with $R/b = (3.0 \div 13.0)$, in which the track diameter $b = (0.8 \div 1.0)$ m. For other values of b, the derived formulas should be treated as a sample estimate of the aerodynamic forces. Reducing the diameter b would reduce the pressure difference on both sides of the thin pipe. The value of the number Re would also decrease, so a completely different calculation model should be made, without the possibility of using the wall functions. It should also be taken into account that the value of the interference factor of fragments of a torus depends on the radius R (as well as on the distance between cylinders). In the case of a torus fragment, the derived formulas are correct only when this fragment tangentially turns into a cylinder, for example, so there are no free ends at which air streams would be detached.

Difficulties in estimating the aerodynamic forces acting on objects of unusual shape result, inter alia, from the fact that the reference surfaces, e.g. of an object in the shape of a half-torus set at different angles to the horizontal, as well as its fragments, do not correspond to the surfaces resulting from the projection of the object on a plane perpendicular to the direction of the wind velocity or the surface of the equivalent cylinder (with the total length of the axis of the half of the torus and the diameter equal to the diameter of the torus track). For example, after adopting the reference surface resulting from the projection of half of the horizontal torus onto the plane perpendicular to the direction of the wind velocity with $w = 11$ m/s, the aerodynamic resistance may be lower even by 22% in relation to the results of the numerical calculations. On the other hand, after assuming the surface resulting from the projection of the torus placed at an angle of 22.5° on the vertical plane perpendicular to the direction of the wind velocity, the aerodynamic resistance at the hurricane wind velocity may increase by 73% in relation to the numerical calculations.

More importantly, objects in the shape of a bent pipe are additionally affected by a horizontal force perpendicular to the aerodynamic drag, which cannot be estimated according to the wind Eurocode. Therefore, in this study, the forces of wind influence on the cylinders and a torus-shaped object were determined and compared.

Similarly to a single cylinder, the airflow around two cylinders is modeled with a length equal to the length of the arc of the quadrant of the torus. Some data and results have been described in the paper [40]. The subject of the analysis is the reactions of individual parts of the cylinders as a result of changes in flow parameters, e.g. pressure. For this purpose, the two cylinders are divided into eight equal parts (see Fig. 14). The cylinders are in tandem arrangement, as well as that the plane containing their axes is yawed at an angle of 45°. The figure shows the directions of the action of the aerodynamic forces and the division of the model into eight parts. The dimensions and FVM mesh are selected analogously to the case of a single cylinder and a torus.

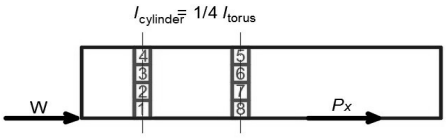

Fig. 14. Longitudinal section of the numerical model of flow around two cylinders and their division into eight parts

As shown in [40], Fig. 15 illustrates the variation of the flow stream near half the torus and the two cylinders in tandem arrangement, aligned horizontally at hurricane wind velocity, when the resultant aerodynamic resistance becomes the integer average. The flow is unsteady and turbulent, but is more symmetric for the cylinders. The track behind the windward cylinder is not closed before the leeward cylinder. However, the aerodynamic resistance increases in relation to the torus. The effect of turbulent and random flow in the vicinity of the leeward half of the torus yawed from the horizontal plane at the angle $\beta = 45°$ continues. Thus, there is a clear influence of the curvature of the torus axis on the pressure and velocity distribution throughout the object. Meanwhile, in the case of two cylinders positioned at the angle $\beta = 45°$ to the direction of the wind velocity and separated by a distance comparable to the double value of the torus radius R, this effect disappears, and the influence of possible in-

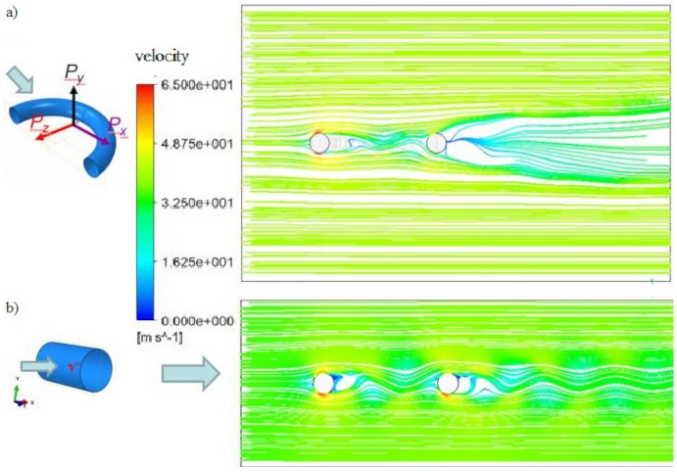

Fig. 15. Distribution of the streamlines in the middle section of the flow: (a) half of the torus positioned horizontally and (b) two cylinders in tandem arrangement, at $w = 33.5$ m/s

terference of velocity fields on the values of aerodynamic forces is negligible. The results of numerical analyses coincide with the classification of the characteristic areas of aerodynamic interference of two cylinders available in the literature (e.g. [41]), according to which the cylinders in the configuration such as in this paper are not subject to interference. They behave differently from, for example, on paper [16].

The graphs in Fig. 16 show the values of the aerodynamic forces in various parts of the torus and cylinders arranged horizontally and at an angle of $\beta = 45°$. The example notation '1-2' on the horizontal axis means a fragment of an object consisting of two parts, and '1-8' – the whole object. The aerodynamic forces on the vertical axis are the total reactions of the analysed part and the previous parts.

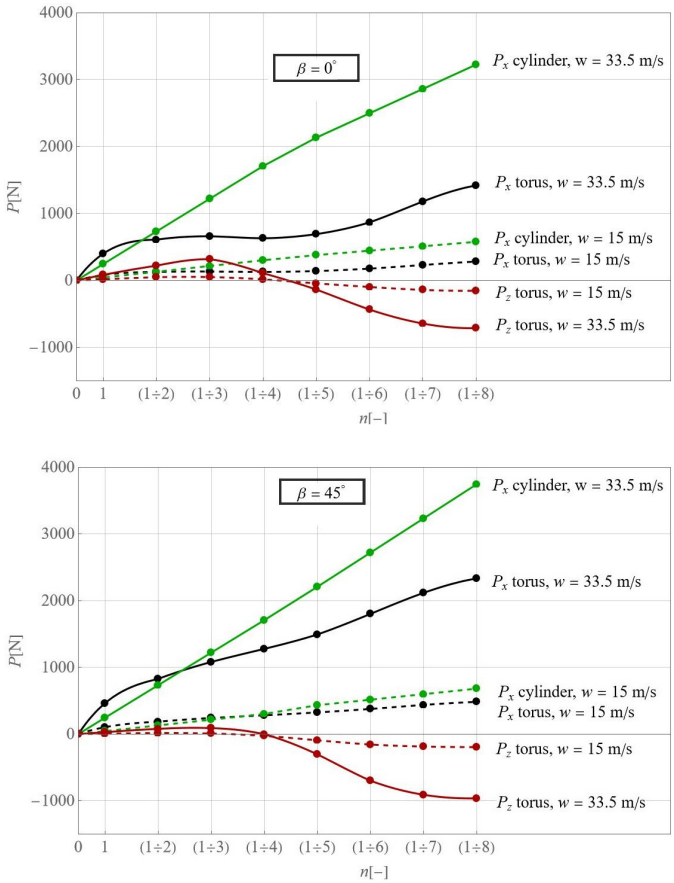

Fig. 16. Dependencies of the total aerodynamic forces of the torus fragments and two cylinders arranged horizontally and at the angle $\beta = 45°$ on the wind velocity w

The graphs show that the value of the drag force of a half of the horizontal torus is approx. 56% lower than the resistance force of two cylinders. On the other hand, the value of the drag force of half the torus yawed at an angle of 45° is approx. 38% lower than the force of two cylinders with an axis connecting their centers yawed at an angle of 45° to the direction of the wind velocity. A more than double reduction of the wind velocity (from 33.5 m/s to 15 m/s) in the half-torus model reduces the aerodynamic drag and the P_z force by approx. 78%.

3. CONCLUSIONS

In this paper, the aerodynamic forces acting on a torus-shaped structure fragment were determined, which is impossible by the existing EN 1991-1-4 standard (the so-called wind standard). These forces were obtained by FSI (force transfer) and UDF methods. It was possible to conclude that the results obtained by the UDF and FSI methods are sufficiently compatible. Using UDF instead of FSI is more convenient and the accuracy of calculations is almost the same. It allowed for the determination of wind forces acting on any part of half of a torus directly in the Fluent and was used as a tool for verifying the analyses of FSI and exact force transfer.

The paper presents new dimensionless graphs: 1) variations of the aerodynamic forces P_x and P_z with the α and β angle using FSI and 2) variations of the total aerodynamic forces P_x and P_z with angle β and velocity of wind w using FSI. They denote the ratio of the value of the aerodynamic force component obtained from numerical analysis to the force that can be calculated analytically. These graphs show that these forces differ by up to three times. Therefore, a function to correct for these force values should be applied. The new formula for estimating the horizontal force P_z perpendicular to the drag force was established. Equations determined in the author's previous papers were verified using additional models of the flow around the halves of a horizontal torus: 1) with a radius $R = 6$ m and a diameter $b = 1$ m and 2) $R = 11$ m and $b = 0.8$ m. P_z force hardly changes after increasing the radius. The action of the wind is the dominant load for the water slide. Variations of the total aerodynamic lift force of the half of the torus with angle β and the velocity of wind w using FSI were presented. It turns out that they almost do not matter in the assessment of structural safety. In addition, useful engineering parameters (such as the pressure distribution and the air velocity field) were determined.

Due to difficulties in estimating the reference surfaces of the object in the shape of a torus, the forces of wind influence on two cylinders and a torus-shaped object were obtained and compared. It turned out that toruses cannot be replaced with two cylinders of a length equal to the length of the arc of the torus quadrant. The value of the drag force of half of the horizontal torus is approximately 56% lower than the resistance force of two cylinders. On the other hand, the value of the drag force of half the torus yawed at an angle of 45° is approximately 38% lower than the force of two cylinders with an axis connecting their centers yawed at an angle of 45° to the direction of the wind velocity. A more than double reduction of the wind velocity (from 33.5 m/s to 15 m/s) in the half-torus model reduces the aerodynamic drag and the P_z force by approximately 78%.

However, the numerical results are influenced by: 1) the precision of numerical models dictated by the lengthy calculations, 2) the adoption of the average value of the drag coefficient in a turbulent flow by the user of the program, 3) changes in the pressure distribution on the walls of the object at different time steps even for the same average value of the drag coefficient, particularly in the area exposed to actions of strong pressure force (fourth, fifth and sixth part of the torus), and 4) the method and quality of approximation of the solutions of the Navier-Stokes and Reynolds equations.

It should be taken into account that the results of numerical analyses are not sufficient to determine the forces acting on the real object. Wind tunnel studies are needed, taking into account the velocity profile near the ground level. A model of, for example, a water slide with a geometry more similar to the real object should be analysed, taking into account the flanges connecting the individual parts and the close location of the ride tracks.

ACKNOWLEDGEMENTS

We gratefully acknowledge Polish high-performance computing infrastructure PLGrid (HPC Centers: ACK Cyfronet AGH, CI TASK, WCSS) for providing computer facilities and support within computational grant no. PLG/2023/016590.

REFERENCES

[1] E. 1991-1-4, "Eurocode 1: Actions on structures -part 1-4: General actions – wind actions," *European Committee for Standardization*, vol. 4, 2005.

[2] A. Padewska, P. Szczepaniak, and A. Wawrzynek, "Oddziaływanie wiatru na obiekt o nietypowym kształcie," *Inżynieria i Budownictwo*, vol. 71, pp. 381–385, 2015, (in Polish).

[3] A. Padewska, "Pogłębiona analiza numeryczna oddziaływania wiatru na obiekty budowlane o nietypowym kształcie i układzie," PhD thesis, Silesian University of Technology, 2016.

[4] A. Padewska, P. Szczepaniak, and A. Wawrzynek, "Analysis of fluid-structure interaction of a torus subjected to wind loads," *Comput. Assist. Meth. Eng. Sci.*, vol. 21, pp. 151–167, 2014. [Online]. Available: https://cames.ippt.gov.pl/index.php/cames/article/view/49

[5] T. Adachi, "The effect of surface roughness of a body in the high Reynolds-number flow," *Int. J. Rotating Mach.*, vol. 2, pp. 23–32, 1995, doi: 10.1155/S1023621X95000170.

[6] A. Roshko, "Experiments on the flow past a circular cylinder at very high Reynolds number," *J. Fluid Mech.*, vol. 10, pp. 345–356, May 1961, doi: 10.1017/S0022112061000950.

[7] J.G.W. Jones and J. Cincotta, "Aerodynamic forces on a stationary and oscillating circular cylinder at high reynolds numbers," 1969.

[8] S. Mingxuan, "Research on the external fluid flow of a round cylinder with CFD," *Highlights Sci. Eng. Technol.*, vol. 37, pp. 309–317, 2022.

[9] S. Hazra, "CFD analysis of steady and transient flow over a cylinder in fluent: A study on von karman vortex shedding," Sep. 2020. [Online]. Available: https://skill-lync.com/student-projects/steady-vs-unsteady-flow-over-a-cylinder-73

[10] L.F.C. de Oliveira and L.J. Pedroso, "Preliminary analysis of flow over a circular cylinder using cfd," in *XLI Ibero-Latin American Congress on Congress on Computational Methods in Engineering*, Nov. 2020.

[11] G.M. Skonecki and J.M. Buick, "Numerical study of flow around two circular cylinders in tandem, side-by-side and staggered arrangements," *Fluids*, vol. 8, p. 148, May 2023, doi: 10.3390/fluids8050148.

[12] X. Yan, R. Carriveau, and D.S. Ting, "Vortical flow structures behind a torus with an aspect ratio of three," *Flow Meas. Instrum.*, vol. 68, p. 101571, Aug. 2019, doi: 10.1016/j.flowmeasinst.2019.101571.

[13] P. Prabhudev, "Investigation of laminar flow inside a torus in openfoam," Master's thesis, KTH Royal Institute of Technology, School of Engineering Sciences, Apr. 2019.

[14] D.M. Subramanian, S. Sanjay, K.K. Sanjay, N. Venkatesh, and Krithicksurya, "Investigate the perform of toroidal propellers using wind tunnel," *Int. Res. J. Adv. Eng. Hub (IRJAEH)*, vol. 2, pp. 1071–1074, Apr. 2024, doi: 10.47392/IRJAEH.2024.0148.

[15] P.W. Bearman, "Circular cylinder wakes and vortex-induced vibrations," *J. Fluids Struct.*, vol. 27, 2011, doi: 10.1016/ j.jfluidstructs.2011.03.021.

[16] E. Błazik-Borowa, A. Flaga, and M. Kazakevič, *Problemy interferencji aerodynamicznej dwóch walców kołowych*. Polska Akademia Nauk, Komitet Inżynierii Lądowej i Wodnej, Instytut Podstawowych Problemów Techniki, Jan. 1997.

[17] A. Borna, W.G. Habashi, G. McClure, and S.K. Nadarajah, "CFD-FSI simulation of vortex-induced vibrations of a circular cylinder with low mass-damping," *Wind Struct.*, vol. 16, pp. 411–431, 2013, doi: 10.12989/was.2013.16.5.411.

[18] S. Kim and H. Sakamoto, "Characteristics of fluctuating lift forces of a circular cylinder during generation of vortex excitation," *Wind Struct.*, vol. 9, pp. 109–124, Apr. 2006, doi: 10.12989/was.2006.9.2.109.

[19] M. Zhao, L. Cheng, H. An, and L. Lu, "Three-dimensional numerical simulation of vortex-induced vibration of an elastically mounted rigid circular cylinder in steady current," *J. Fluids. Struct.*, vol. 50, pp. 292–311, Oct. 2014, doi: 10.1016/j.jfluidstructs.2014.05.016.

[20] A. Padewska-Jurczak, P. Szczepaniak, and Z. Buliński, "Numerical determination of wind forces acting on structural elements in the shape of a curved pipe," *Wind Struct.*, vol. 30, pp. 15–27, 2020, doi: 10.12989/was.2020.30.1.015.

[21] Y. Inouel, S. Yamashita, and M. Kumada, "An experimental study on a wake of a torus body using uvp," in *1st International Symposium on Ultrasonic Doppler Methods for Fluid Mechanics and Fluid Engineering- ISUD*, 1996.

[22] A.D. Vecchi, "Wake dynamics of flow past a curved circular cross-section body under cross-flow vibration," Ph.D. dissertation, University of London, 2009.

[23] A. Miliou, S. Sherwin, and J. Graham, "Wake topology of curved cylinders at low reynolds numbers," *Flow Turbul. Combust.*, vol. 71, pp. 147–160, 2003, doi: 10.1023/B:APPL.0000014920.94050.a2.

[24] P. Szczepaniak and A. Padewska, "Wind load of a curved circular cylinder structures," in *12th International Conference on New Trends in Statics and Dynamics of Buildings*, N. Jendzelovsky and A. Grmanova, Eds. Bratislava: Slovak University of Technology, 2014, pp. 517–530.

[25] ANSYS Inc., "Ansys documentation for release 15/customer training material," 2013. [Online]. Available: https://www.ansys.com/academic/learning-resources

[26] Dassault Systemes, "Introduction to Abaqus/CFD," 2010.

[27] T. Jiyuan, Y. Guan-Heng, and L. Chaoqun, *Computational Fluid Dynamics, Second Edition; A Practical Approach*. Butterworth-Heinemann, 2019.

[28] F.R. Menter, "Two-equation eddy-viscosity turbulence models for engineering applications," *AIAA J.*, vol. 32, pp. 1598–1605, Aug. 1994, doi: 10.2514/3.12149.

[29] J.H. Lienhard, *Synopsis of Lift, Drag, and Vortex Frequency Data for Rigid Circular Cylinders*. College of Engineering, Research

DivisionTechnical Extension Service, Washington State University, 1966.

[30] J. Anderson, *Computational Fluid Dynamics: The Basics with Applications. 1995*. McGrawhill Inc, 1995.

[31] H. Versteeg and W. Malalasekra, *An Introduction to Computational Fluid Dynamics: The Finite Volume Method-2nd Edition*. Prentice Hall, 2007, vol. 43.

[32] D.C. Wilcox, "Turbulence modeling for CFD (third edition)," *DCW Industries*, 2006.

[33] K. Suga, T. Craft, and H. Iacovides, "Extending an analytical wall-function for turbulent flows over rough walls," in *Engineering Turbulence Modelling and Experiments 6*, W. Rodi and M. Mulas, Eds. Amsterdam: Elsevier Science B.V., 2005, pp. 157–166, doi: 10.1016/B978-008044544-1/50014-5.

[34] P. Catalano, M. Wang, G. Iaccarino, and P. Moin, "Numerical simulation of the flow around a circular cylinder at high reynolds numbers," *Int. Journal Heat Fluid Flow*, vol. 24, pp. 463–469, Aug. 2003, doi: 10.1016/S0142-727X(03)00061-4.

[35] A. Flaga, *Inżynieria wiatrowa. Podstawy i zastosowania*. Arkady, 2008.

[36] K. Warschauer and J. Leene, "Experiments on mean and fluctuating pressures of circular cylinders at cross flow at very high reynolds number," in *Proc. International Conference on Wind Effects on Buildings and Structures*, 1971, pp. 305–315.

[37] M. Zdravkovich, *Flow Around Circular Cylinders. Volume 2: Applications*. Oxford University Press, 2003.

[38] Y. Bazilevs, K. Takizawa, and T.E. Tezduyar, *Computational Fluid–Structure Interaction*. Wiley, Jan. 2013, doi: 10.1002/9781118483565.

[39] A. Noorani, G.E. Khoury, and P. Schlatter, "Evolution of turbulence characteristics from straight to curved pipes," *Int. J. Heat Fluid Flow*, vol. 41, pp. 16–26, 2013.

[40] A. Padewska, P. Szczepaniak, and A. Wawrzynek, "Porównanie sił aerodynamicznych działających na połowę torusa i dwa walce o tej samej długości," *Modelowanie Inżynierskie*, vol. 29, pp. 52–57, 2016.

[41] M. Zdravkovich, "Review of interference-induced oscillations in flow past two parallel circular cylinders in various arrangements," *J. Wind Eng. Ind. Aerodyn.*, vol. 28, pp. 183–199, Aug. 1988, doi: 10.1016/0167-6105(88)90115-8.